The distribution of density in supersonic turbulence

Jonathan Squire[1,2] & Philip F. Hopkins[1]

[1]*TAPIR, Mailcode 350-17, California Institute of Technology, Pasadena, CA 91125, USA*
[2]*Walter Burke Institute for Theoretical Physics, Pasadena, CA 91125, USA*

ABSTRACT
We propose a model for the density statistics in supersonic turbulence, which play a crucial role in star-formation and the physics of the interstellar medium (ISM). Motivated by [Hopkins, MNRAS, **430**, 1880 (2013)], the model considers the density to be arranged into a collection of strong shocks of width $\sim \mathcal{M}^{-2}$, where $\mathcal{M}$ is the turbulent Mach number. With two physically motivated parameters, the model predicts all density statistics for $\mathcal{M} > 1$ turbulence: the density probability distribution and its intermittency (deviation from log-normality), the density variance–Mach number relation, power spectra, and structure functions. For the proposed model parameters, reasonable agreement is seen between model predictions and numerical simulations, albeit within the large uncertainties associated with current simulation results. More generally, the model could provide a useful framework for more detailed analysis of future simulations and observational data. Due to the simple physical motivations for the model in terms of shocks, it is straightforward to generalize to more complex physical processes, which will be helpful in future more detailed applications to the ISM. We see good qualitative agreement between such extensions and recent simulations of non-isothermal turbulence.

Key words: star formation: general — turbulence — shock waves — ISM: kinematics and dynamics

1 INTRODUCTION

A detailed knowledge of gas statistics in the interstellar medium (ISM) is pivotal for theories of star formation and the stellar initial mass function (see, for example, Krumholz & McKee 2005; Federrath & Klessen 2012; Hopkins 2013a; Hennebelle & Chabrier 2013 and references therein). The difficulty in understanding these statistics arises because much of the ISM is in a state of *supersonic turbulence*—a highly chaotic tangle of interacting shocks with structure spanning an enormous range in scale. However, despite a wide range of work on the subject, enabled in large part by the explosive growth in computational power (e.g., Kritsuk et al. 2007; Lemaster & Stone 2008; Molina et al. 2012; Federrath 2013; Pan et al. 2016 and references therein), much less is known about the statistical properties of supersonic turbulence in comparison to its subsonic cousin (Federrath 2013; Pan et al. 2016). For example, despite some promising results (e.g., Boldyrev 2002; Aluie 2011; Banerjee & Galtier 2013), we currently lack a well-accepted theory for the velocity power spectrum, similar to the standard Kolmogorov phenomenology for subsonic turbulence (Kolmogorov 1941). Further, an important aspect of supersonic turbulence theory, which is much less relevant in subsonic turbulence, is the density statistics. These are crucial for star-formation applications and directly observable in the ISM. However, although there are certain well-established results—most importantly the *density variance–Mach number relation*: that the density distribution is approximately log-normal with a variance that increases with Mach number (Passot & Vázquez-Semadeni 1998; Price et al. 2011; Padoan & Nordlund 2011; Molina et al. 2012; Federrath & Banerjee 2015; Pan et al. 2016)—we lack detailed understanding of many important issues. For example, the power spectrum of density and its variation with Mach number is not well understood (Kim & Ryu 2005; Kritsuk

et al. 2007; Kowal et al. 2007; Konstandin et al. 2016). Further, an important limitation of the density variance-Mach number relation is that the density can be quite *intermittent*, viz., it is not distributed log-normally. This behavior manifests itself in a significant negative skewness in the probability density function (PDF) (Federrath et al. 2008; Price & Federrath 2010; Schmidt et al. 2009; Konstandin et al. 2012; Hopkins 2013b), enhancing the probability of low density regions while decreasing the probability of high density regions. The purpose of this work is to propose and examine a simple phenomenological model for the turbulent density field that encompasses all such statistics: the power spectrum, the density PDF and intermittency, and how these vary with turbulent Mach number.

It is worth elaborating on the density intermittency mentioned in the previous paragraph: is this important, or simply a formal nuisance to occupy the idle theorist? For some applications, in particular those that depend on events that occur regularly (i.e., with high probability), the answer is probably that intermittency is not important: so long as the density PDF is approximately log-normal near its peak, high-probability events will be well-characterized purely by the variance. However, many physically interesting properties that one might wish to derive from turbulent PDFs involve rare events, in particular those involving high-density regions. As a simple example, if we were interested in regions with a factor ~ 100 enhancement in density over the mean at a turbulent Mach number $\mathcal{M} \sim 15$ (e.g., to push the density above the Jean's density and enable gravitational collapse), the probability of finding such a region could easily be over-estimated by 1 to 3 orders of magnitude by a log-normal model, compared to a more realistic intermittent model with the same variance. Gaining a better understanding of the density PDF can also be motivated by other more fundamental interests. For instance, averaged over scale l, the PDF of the density

field *cannot* be log-normal (note that l could be the grid scale here): by predicting a nonzero probability of finding densities greater than the ratio between the box volume and l^3, a log-normal PDF violates mass conservation (see also Hopkins 2013b; hereafter H13). Further, we shall find that the process of understanding the origin of the density intermittency using the properties of shocks leads to various other insights; for example, the origins of the qualitatively different PDF shapes seen in non-isothermal or magnetohydrodynamic (MHD) turbulence.

This work involves an extension of the supersonic density PDF model proposed by H13 to multi-point statistics. Specifically, this involves specifying the properties of the PDF *as a function of scale*, viz., after averaging the density field over scale l (which is some fraction of the box scale L) what is its PDF? Such a model completely specifies the statistical properties of the turbulent density field and contains significantly more information than the 1-point PDF that is usually calculated from numerical studies. For example, it allows the prediction of the density variance-Mach number relation, a similar relation for the intermittency, density power spectra, and structure functions. Further, these predictions are made with just one or two physically motivated free parameters, that are independent of Mach number $\mathcal{M}$ once this is large. Extending the discussions in H13 and based on She-Leveque intermittency models that have been successful for subsonic turbulence (She & Leveque 1994; She & Waymire 1995; Dubrulle 1994; Castaing 1996; He et al. 1998), the model relies on a simple physical picture in which the density field is made up of a series of shocks covering a wide range of scales down to where the turbulence becomes subsonic. Starting from the box scale, at which the density field is simply constant, the shocks add density variance in the form of discrete multiplicative events, where the size of individual events is related to the physical properties of a shock. This predicts a strong relationship between the size of individual events—which controls the intermittency— and the variance of the density PDF, governed by the range of scales (i.e., L/l) and the Mach number. Comparison to various well-known results and trends, as well as our own numerical simulations, illustrates reasonable agreement across a range in Mach numbers. In addition, given the simple physical reasoning used to derive model parameters from isothermal shock properties, we extend the model to more complex and realistic physics—for example, a non-isothermal gas equation of state, or MHD—explaining various aspects of the density PDFs and why these are different from isothermal turbulence.

The remainder of the paper is organized as follows. In Sec. 2, we outline a few general considerations that will be used to motivate various choices in our model. In Sec 3 we explain the model, in particular how the mathematical structure of a (compound) log-Poisson random process can be related to the properties of individual shocks. We take particular care here to outline the choices necessary for various parameters, and how these may be motivated or phenomenologically derived from physical properties of the turbulence. We then outline a variety of predictions of the model—including the density variance–Mach number relation, intermittency predictions, and power spectra—and compare these to numerical simulations. This comparison involves both previous results and a variety of new simulations using the Lagrangian Meshless-Finite-Mass method in the GIZMO code (Hopkins 2015a), which we use to directly compute the density PDF as a function of scale. We also measure the physical size of shock structures, which forms an important part of our argument, in App. B. Overall, model predictions seem to match with numerical results up to numerical uncertainties, although more detailed comparisons

will be necessary to understand its successes and failures more completely. We finish with an extension to non-isothermal turbulence (illustrating reasonable qualitative agreement with the simulations of Federrath & Banerjee 2015) and a discussion of MHD, before concluding by reiterating the model's main predictions.

2 GENERAL CONSIDERATIONS

Before continuing, it seems worth enumerating several general points about supersonic turbulence. While some of these are well known, given that each plays some crucial role in the derivation of our model, it is helpful to clearly explicate these ideas early on in our discussion.

(i) Supersonic turbulence is not scale invariant, except in the infinite Mach number limit. This arises because of the importance of the sonic scale l_{sonic}, which is the scale at which $v_l = v_{|l|} = \langle |v(x+l) - v(x)| \rangle \sim c_s$; i.e., the scale at which the turbulence becomes subsonic. For modest Mach numbers common in nature or numerical experiments, the scale separation between l_{sonic} and the driving scale is also modest, challenging the relevance of the concept of a supersonic "inertial range." This feature necessarily leads to some important differences in the theoretical treatment of supersonic turbulence in comparison to subsonic turbulence.

(ii) Since density is effectively defined with reference to a volume (it is the mass per unit volume), the density itself, and its PDF, are naturally defined with reference to an averaging scale. This density PDF as a function of scale encodes a wide variety of useful statistical information about the density field. By only ever studying the PDF with respect to some arbitrary scale (usually the grid scale in numerical simulations), one risks missing important trends or effects, particularly considering that the sonic scale is often close to the grid scale for Mach numbers of $\sim 10 \rightarrow 20$ at currently available numerical resolutions (see point 1). As an example, in the numerical simulations in this work, we find that the density PDF becomes significantly *less* intermittent below l_{sonic}, presumably because the density field on subsonic scales involves nearly Gaussian fluctuations (Federrath et al. 2010; Konstandin et al. 2012). The density averaged over scale is also relevant for applications, being an important quantity for studying gravitational collapse. For example, a region is of (linear) size l is unstable to collapse if l is larger than the Jean's length

$$\lambda_J \sim \frac{c_s}{\sqrt{G\rho_l}}. \tag{1}$$

Here ρ_l is the average density over l, so to understand the statistics of gravitational collapse in a turbulent cloud, we require an understanding of the density PDF as a function of scale.

(iii) A PDF that appears more log-normal does not necessarily imply that the underlying statistics are closer to Gaussian. Instead, the apparent Gaussianity of the PDF may be a result of the suppression of low densities compared to the isothermal case. This point is important for MHD and non-isothermal turbulence.

(iv) The assumption that the shock width is equal to the sonic scale—while useful as a phenomenological tool for deriving density variance–Mach number relations (Price et al. 2011; Padoan & Nordlund 2011; Molina et al. 2012; Federrath & Banerjee 2015)—is inconsistent with log-normal density statistics. In particular, for isothermal shocks with a density contrast $\sim \mathcal{M}^2$, such a model involves *all* of the mass being concentrated in a single shock, which leads to an unphysically intermittent density distribution. In our model, we take the shock width to be some small fixed fraction

κ of l_{sonic}, and it will transpire that the κ parameter controls the intermittency. The success of density variance estimates using l_{sonic} as the shock width may then be related to κ being approximately universal, even in more complex physical situations (e.g., MHD).

(v) The infinite-Mach-number limit is not equivalent to Burger's turbulence (where the pressure term is neglected in the Navier-Stokes equations). This is because there are always some regions, no matter how large $\mathcal{M}$, where the pressure forces becomes important; see Passot & Vázquez-Semadeni (1998).
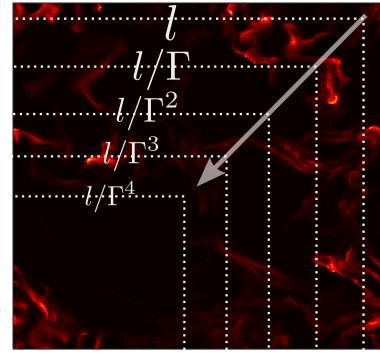
3 MODEL DESCRIPTION

In this section we describe the mathematical structure and physical motivation for the density model. We shall denote the scale over which the density is averaged as l, the box scale as L, the PDF of the density averaged over scale l as $\mathcal{P}_l(\rho)$, and assume that the volume average of ρ over the whole box is $\langle\rho\rangle = M/L^3 = 1$. Start by considering the density averaged over the scale of the box $l = L$, which by definition is $\rho = 1$ with the PDF $\mathcal{P}_L(\rho) = \delta(\rho - 1)$. The model then provides a description of the density PDF averaged over successively smaller subvolumes of the box, $\mathcal{P}_l(\rho)$, a full knowledge of which effectively provides a full description of the statistical state of the turbulent density field.

This process is described mathematically by a series of N steps, each of which decrease the volume over which ρ is averaged by a factor $\Gamma > 1$, such that $l^3 = L^3/\Gamma^N$. The basic idea is that as one makes a jump down in scale from l to l/Γ, there is some probability, scaling with $\Gamma - 1$, of an "event" that changes the density by $\delta\rho$. This event will be related to a shock structure that was previously in the larger volume (at scale l) being lost from the smaller volume (at scale l/Γ), thus causing a decrease in density in the volume being considered. This shock is related to velocity and density structures that vary over scale l, since smaller structures cannot contribute significantly due to their smaller size, while there are too few larger structures (since these vary over scales $\gg l$). The size of this "jump" decrease in density $\delta\rho$ is related to the proportion of mass that resides in the shock that is lost in the step, and is itself a random variable. Assuming that most of the mass in the system is tied up in shocks, steps with no event will cause the average density to increase slightly, because the density in the volume that is lost in the step is less than the average density in the system. We graphically illustrate such a process in Fig. 1, showing how in a volume filled with high density shocks, some steps will cause a large decrease in the mass enclosed by the new volume (i.e., an event), while other steps will not (no event).

3.1 Compound-log-Poisson cascades

The process we have just described is known mathematically as a *compound-log-Poisson* random process. Such processes are well characterized and have been particularly successful in phenomenological turbulence intermittency models for velocity structure functions (She & Leveque 1994; Dubrulle 1994; Castaing 1996; He et al. 1998; Boldyrev 2002; Mallet & Schekochihin 2017). The process occurs in log space because we consider multiplicative changes to the volume and density (which are additive in log space), while it is a Poisson process because the probability of an event is proportional to the size of the jump in volume (with infinitesimally small jumps being considered). If the size of each density jump,

Figure 1. Cartoon of how the average density on scale l can change as l decreases, projected into the 2-D plane. The brightness illustrates the density field, which is dominated by thin shock structures with a large proportion of the total mass. In the hypothetical step in scale from l to l/Γ the difference in volume (between the squares) covers a very high density shock region (upper right), implying the average density at scale l/Γ is *less* than that at l, since a significant proportion of the mass is lost in the jump. In contrast, in the jump from l/Γ to l/Γ^2, which entails the same proportional volume change, there is not a significant change in density because all high density regions remain inside the new volume at scale l/Γ^2.

$\ln\rho \to \ln\rho - \delta\ln\rho$, is fixed (i.e., if $\delta\ln\rho$ is a number), then the resulting distribution will be log-Poisson,

$$\mathcal{P}(\ln\rho) = \frac{\lambda^{-\ln\rho + \Upsilon}e^{-\lambda}}{(-\ln\rho + \Upsilon)!}, \tag{2}$$

where the Υ accounts for a mean shift in the distribution (required to keep $\langle\rho\rangle = 1$; see below). However, the distribution (2) has the unphysical property of being discrete, since the jump sizes are discrete, and is thus somewhat inconvenient as a model for density. This issue may be circumvented by postulating that the size of each jump $\delta\ln\rho$ is itself a random variable, with probability distribution $\delta\ln\rho \sim \mathcal{P}_\delta(\delta\ln\rho)$. This leads to a "compound-log-Poisson" distribution, where "compound" refers to the idea that the distribution is formed as a random process of a random variable. Following H13, we take the jump sizes to be distributed exponentially (Castaing 1996),

$$\mathcal{P}_\delta(\delta\ln\rho) = \begin{cases} T^{-1}\exp[(\delta\ln\rho - \epsilon)/T] & \delta\ln\rho - \epsilon < 0 \\ 0 & \delta\ln\rho - \epsilon > 0 \end{cases}, \tag{3}$$
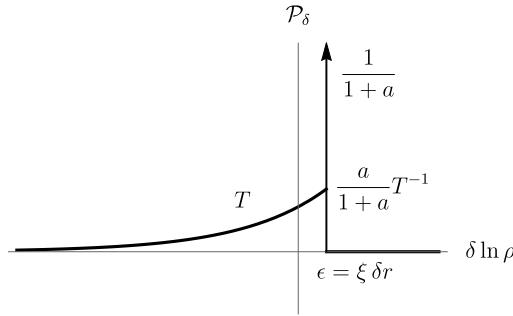
where T is the mean jump size and ϵ is a constant that is used to ensure $\langle\rho\rangle = 1$; see Fig. 2. This leads to a convenient form for the PDF that matches density PDFs measured from simulations remarkably well (H13).[1]

We now derive the PDF of $\ln\rho$, $\mathcal{P}_l(\ln\rho)$. that arises from this process. Assuming that the parameter T does not depend on scale, $\mathcal{P}_l(\ln\rho)$ is the convolution of n $\mathcal{P}_\delta$ distributions shifted by the total number of steps $\Upsilon = N\epsilon$,

$$\mathcal{P}_l(\ln\rho) = \mathcal{P}_\delta^{\otimes n} = \text{Gamma}(-\ln\rho + \Upsilon; n, T), \tag{4}$$

where $\cdot^{\otimes n}$ denotes the convolution power and $\text{Gamma}(x; n, T) =$

---

[1] The choice of an exponential distribution for $\mathcal{P}_\delta(\delta\ln\rho)$ can be motivated as the only choice other than a delta-function distribution (i.e., a standard log-Poisson process) that leads to a single fractal dimension for the most singular structures (He et al. 1998). However, since the system we model is not scale invariant anyway, our motivation for this choice is primarily simplicity—the PDF may be written in a simple closed form without unphysical discrete jumps—and other choices give similar results.

Figure 2. The PDF for a single step in the cascade, which is $a(1+a)^{-1}\mathcal{P}_\delta(x)+(1+a)^{-1}\delta(x)$, where a is a small parameter proportional to the size of the step in volume $\delta r = \ln(\Gamma - 1)$. The maximum ϵ is chosen as $\epsilon = \xi\delta r$, which correctly captures the true maximum of ρ when $\xi = 3$, and otherwise describes how the maximum density changes with scale. When coupled with the constraint $\langle\rho\rangle = 1$, ξ sets the proportionality between a and δr as $a = \xi\delta r(1+T)T^{-1}$.

$x^{n-1}e^{-x/T}T^{-n}\Gamma(n)^{-1}$ is the Gamma distribution. As one takes the limit $N \to \infty$, $\Gamma \to 1$ with $N(\Gamma-1) = \lambda$, the number of events n is itself is a Poisson-distributed random variable with mean λ (this will depend on scale l and is specified below), so the full PDF for $\ln\rho$ is simply a sum of the PDFs for a given n, weighted by the probability that such an n occurs $n \sim \lambda^n e^{-\lambda}/n!$. Putting this together, one obtains

$$\ln\rho \sim \mathcal{P}_l(\ln\rho) = \sum_{n=0}^{\infty}\frac{\lambda^n e^{-\lambda}}{n!}\frac{u^{n-1}}{T\Gamma(n)}\exp(-u)$$

$$= T^{-1}\sqrt{\frac{\lambda}{u}}I_1(2\sqrt{u\lambda})\exp[-(\lambda+u)], \qquad (5)$$

where $u \equiv (-\ln\rho + \Upsilon)/T$, $I_1(x)$ is the first-order modified Bessel function of the first kind, and $\mathcal{P}_l(\ln\rho)$ is nonzero only for $u > 0$. We may then fix $\Upsilon = N\epsilon = \lambda T(1+T)^{-1}$ using the constraint $\langle e^{\ln\rho}\rangle = \langle\rho\rangle = 1$, which leads to the density PDF proposed in H13. The volume-weighted variance is $S_{\ln\rho,V} = 2\lambda T^2$, while T—the mean size of the jumps—is an intermittency parameter that skews the distribution towards higher probability at $\ln\rho < 0$. In line with our intuition, small numbers of large density jumps (e.g., large shocks) lead to highly intermittent distributions, while a large number of small jumps leads to distributions that are very close to log-normal. The mass-weighted variance is $S_{\ln\rho,M} = 2\lambda T^2(1+T)^{-3}$, so $S_{\ln\rho,M} = S_{\ln\rho,V}$ in the $T = 0$ (log-normal) limit as expected (H13). Also note that, unlike a log-normal PDF, this distribution has a maximum value $\ln\rho = \Upsilon$ above which $\mathcal{P}_l(\ln\rho) = 0$. This property is entirely physical: the probability of encountering $\rho > \langle\rho\rangle(L/l)^3$ is identically zero, since there is not enough mass in the system.

To relate the mathematical model (5) to the physical properties of supersonic turbulence, we require two extra pieces of information: (i) how the average number of events λ relates to the physical scale l, and (ii) how the parameter T (the size of an event) relates to the physical properties of a shock structure. We tackle these issues in the next two sections.

3.2 Variation with scale and mass conservation

In this section, we relate the average number of events λ to the physical scale l. To explore this, it is helpful to consider the PDF of $\delta\ln\rho$ for a single step, which is illustrated in Fig. 2. This is a mixture distribution of $\mathcal{P}_\delta$ with probability $a/(1+a)$ (there is

an event), and a (shifted) δ-function distribution with probability $1/(1+a)$ (there is no event). The parameter a thus determines the mean number of events over a given number of steps, implying the relation between λ and l is controlled by the proportionality constant between a and the (log) differential change in scale between l and l/Γ, $\delta r = \ln\Gamma \approx \Gamma - 1$.

The first constraint we can apply to the single-step PDF is that the total mass must conserved, $\langle\delta\rho\rangle_\delta = \langle e^{\delta\ln\rho+\epsilon}\rangle_\delta = 1$ (where $\langle\cdot\rangle_\delta$ indicates the mean over the single-step PDF). This leads to the constraint

$$a = \epsilon\frac{1+T}{T}. \qquad (6)$$

The second mass-conservation-related constraint we apply is that the *maximum* density scales as $(L/l)^\xi$; i.e., $\epsilon = \xi\delta r$, or

$$\lambda_l = Na = \xi\frac{1+T}{T}\ln\left(\frac{L}{l}\right). \qquad (7)$$

This constraint simply states that the increase in density when there is no event is proportional to some power of the change in linear dimension. If $\xi = 3$, this implies that *all* of the mass from the old volume is contained into the new volume when there is no event, which will give a density PDF with the true (physical) density maximum $\rho_{\max} = (L/l)^3$. However, we find empirically (see Sec. 4) that $\epsilon = 3\delta r$ predicts a PDF that is insufficiently intermittent, and that $\epsilon \approx 1.5\delta r$ provides a closer fit to data[2] (for the model of T proposed in Sec. 3.3 below). We thus consider ξ to be a parameter of our model, which should be universal for all turbulence with $\mathcal{M} \gg 1$. Note that a deviation from this general form (i.e., if ϵ was not taken proportional to δr but chosen through some other method) would imply that the geometrical properties and distribution of the shocks was a function of scale. This would be inconsistent with the existence of an inertial range in the $\mathcal{M} \gg 1$ limit, but could in principle occur for $\mathcal{M} \sim 1$.

3.3 Relating T to the size of a shock

In this section, we relate the intermittency parameter T to the physical properties of individual shocks (see also H13 appendix). In the moderate-$\mathcal{M}$ regime, which is both physically relevant and most commonly probed by current numerical simulations, the system is not scale invariant and T must be an increasing function of $\mathcal{M}$, eventually asymptoting to some value $T \lesssim 1$.[3] Here we propose a simple physically motivated model, which gives a good match to simulations (see Sec. 4), is easily extendable to other equations of state (see Sec. 5) and is based on well-accepted ideas put forth in previous literature (Passot & Vázquez-Semadeni 1998; Price et al. 2011; Padoan & Nordlund 2011; Molina et al. 2012). However, a

[2] Although it is difficult motivate a particular value for ξ, a value $\xi < 3$ fits our intuitive picture of a collection of shocks. In particular, even in the case when all of the mass is contained in infinitely thin shocks, most of these will be at some angle to the changing volume and thus a "no event" step will involve losing a small part of this mass. For example, if such shocks on average intersect one dimension of the changing volume, this would imply $\xi = 3 - 1 = 2$, while if they intersect two it would imply $\xi = 3 - 2 = 1$. Thus, ξ is related to the density in unshocked regions, the dimensionality of the shocks, and their distribution in angle.
[3] Note that $T > 1$ implies most of the mass in the system is contained in a single shocked structure, which might cause one to question whether the system is truly turbulent.

variety of other possibilities exist, some of which could prove similarly successful and also be physically motivated. This is discussed further in Sec. 3.5.

"Shocks" will be taken as regions that are extended across the volume being considered (i.e., of size l) in two-dimensions, and be of small but finite extent in the other dimension (Federrath et al. 2008). Concentrating for now on the simplest isothermal equation of state, the Rankine-Hugoniot conditions for mass and momentum conservation of ρ and v on either side of a shock are

$$\rho_1 v_{c1} = \rho_2 v_{c2}, \quad \rho_1(v_{c1}^2 + c_s^2) = \rho_2(v_{c2}^2 + c_s^2), \tag{8}$$

where v_{ci} is the velocity on side i in the direction perpendicular to the shock. Solution of Eq. (8) with $v_{c0} = b\mathcal{M}c_s$, based on some average Mach-number $\mathcal{M}$ and average fraction of the velocity in compressive modes b (Padoan et al. 1997; Passot & Vázquez-Semadeni 1998; Federrath et al. 2008), leads to an approximate relation for the density contrast:

$$\frac{\rho_1}{\rho_0} \sim b^2\mathcal{M}^2. \tag{9}$$

As common in previous works (Lemaster & Stone 2008; Padoan et al. 1997; Passot & Vázquez-Semadeni 1998), we use Eq. (9) to relate the density in a shock to that outside the shock, for each scale in the turbulence.

The important quantity controlling T is the average density jump that occurs when a shock is removed from the volume being considered. This depends on both the density contrast and the volume of shocks, which requires a measure of their physical width r_{shock}. Given that there is only one scale in the system—the sonic scale l_{sonic}, at which $v \sim c_s$—we effectively have only one choice: that the shock has width κl_{sonic}, with $\kappa < 1$ some arbitrary parameter. Denoting v_l as the approximate velocity difference across scale l and taking $v_l \sim (l/L)^\zeta \mathcal{M}c_s$ with $\zeta \sim 1/2$ (i.e., a velocity power spectrum $E \sim k^{-1/\zeta}$; Federrath 2013), one obtains $l_{\text{sonic}}/L \sim \mathcal{M}^{-2}$. Given the scaling of the density contrast Eq. (9), we see that this prescription $r_{\text{shock}} \sim \kappa l_{\text{sonic}}$, states that a fixed fraction of the mass ($\sim \kappa b^2$) is contained in individual shocks in the high-$\mathcal{M}$ limit.

Denoting the density in the shock ρ_{shock}, the density outside the shock ρ_{out}, and the average density over both regions ρ_{av}, we see from Eq. (3) that

$$T \approx \ln\frac{\rho_{\text{out}}}{\rho_{\text{av}}} \tag{10}$$

(where we have neglected the offset ϵ since δr may be taken to be small). If we then take $\rho_{\text{shock}} \sim \mathcal{M}^2 \rho_{\text{out}}$ (absorbing b into κ),[4] then from mass conservation (where $V = l^3$ is the volume),

$$\rho_{\text{out}}(V - V_{\text{shock}}) + \rho_{\text{shock}}V_{\text{shock}} = V\rho_{\text{av}}, \tag{11}$$

and $V_{\text{shock}} \sim \kappa l_{\text{sonic}} l^2$, we obtain

$$T \sim \kappa(1 - \mathcal{M}_l^{-2}) = \kappa\left(1 - \frac{L}{l}\mathcal{M}^{-2}\right), \tag{12}$$

assuming small κ.

We thus have a simple connection between the mathematical

log-Poisson cascade described above and the physical size and density structure of shocks. It is worth noting that, given the isothermal shock jump relation, making the assumption "shock width $\sim l_{\text{sonic}}$" (without some extra factor $\kappa < 1$) is technically inconsistent with Gaussian statistics, although it is often used to estimate the density variance (Padoan & Nordlund 2011; Molina et al. 2012; Federrath & Banerjee 2015). Systems with a larger proportion of the mass in a small number of shocks will have more intermittent statistics, since T controls the deviation from Gaussianity in Eq. (5). In App. B we measure the shock sizes from simulation, finding reasonable agreement with the hypothesis that they scale as some fraction of l_{sonic} (see Fig. B1). Finally, we note that since we consider only density changes arising from shocks, we are explicitly neglecting all scales $l < l_{\text{sonic}}$ where $\mathcal{M} \lesssim 1$; that is, the property $T(\mathcal{M}_l < 0) = 0$ is a consequence of our focus on shocks as drivers of density change and is not physical. Of course, subsonic motions do cause variation in density, and a model for $T(\mathcal{M} < 1)$ could be added to the supersonic model presented here if so desired (Federrath et al. 2010).

3.4 The model

We have now completely specified the full, scale-dependent statistics for the density field. Assuming for the moment that $T = \kappa$ is constant for $l > l_{\text{sonic}}$ [this is true for $\mathcal{M} \gtrsim 5$; see Eq. (12)], we obtain a simple, two-parameter (κ and ξ) model for the density PDF as a function of scale

$$\ln\rho \sim \mathcal{P}_l(\ln\rho) \approx T^{-1}\sqrt{\frac{\lambda}{u}}I_1(2\sqrt{u\lambda})\exp[-(\lambda+u)],$$
$$\lambda = \xi\left(1 + \frac{1}{T}\right)\ln\left(\frac{L}{l}\right), \quad T = \kappa,$$
$$u = -\ln\rho + \xi\ln\left(\frac{L}{l}\right) \quad (\text{with } u > 0), \tag{13}$$

for $l > l_{\text{sonic}} = L\mathcal{M}^{-2}$. For $l < l_{\text{sonic}}$, we take $\mathcal{P}_l(\ln\rho) = \mathcal{P}_{l_{\text{sonic}}}(\ln\rho)$; that is, we neglect the subsonic contribution, which is minor for $\mathcal{M} \gg 1$ (Federrath et al. 2010). Note that the Mach number dependence is implicit in Eq. (13) through the dependence on l_{sonic}, since higher $\mathcal{M}$ will lead to larger L/l with $l > l_{\text{sonic}}$, and thus larger λ. The difference between compressible and solenoidal large-scale motions (e.g., due to forcing; Schmidt et al. 2009; Federrath 2013) is absorbed into the parameter κ that controls the width and density contrast of individual shocks.

Since T is not truly constant, the functional form of the PDF will differ somewhat from Eq. (13). In fact, even the H13 form [Eq. (5)] is not produced by the model with scale-dependent T, since the PDF of each step varies with l. While in principle one needs to take the convolution of a series of distributions $\mathcal{P}_\delta(\delta\ln\rho; T)$ with differing T, this is analytically unfeasible. Instead, the true PDF can be well approximated by taking the same algebraic form of the PDF Eq. (5), with mean and variance calculated from the true random process (Stewart et al. 2006; Hopkins 2015b). This gives

$$T_l = \frac{\int_{\ln l}^{\ln L} T(l')[1 + T(l')]d\ln l'}{\int_{\ln l}^{\ln L}[1 + T(l')]d\ln l'},$$
$$\lambda_l = \frac{\left(\int_{\ln l}^{\ln L}[1 + T(l')]d\ln l'\right)^2}{\int_{\ln l}^{\ln L} T(l')(1 + T(l'))d\ln l'}, \tag{14}$$

where T_l and λ_l are the "averaged" values to use in the PDF Eq. (13), while $T(l) = \kappa(1 - \mathcal{M}_l^{-2}) = \kappa(1 - \mathcal{M}^{-2}L/l)$ is the "local"

---

[4] We thus expect κ to differ between compressibly and solenoidally forced turbulence (Federrath 2013). Of course, b and κ are not quite equivalent, relating to the shock density contrast and volume respectively. Nonetheless, retaining b separately leads to nearly the same relation as Eq. (12) (with $\kappa \to b^2\kappa$), but with unphysical ($T < 0$) behavior near $\mathcal{M} = 1$. In any case, κ and b are each based on heuristic ideas, and assigning too much physical relevance to the details of this model is not particularly productive.

value of T taken from the shock model. Although the integrals in Eq. (14) are straightforward analytically, the added complexity makes these forms inconvenient except for plotting. In any case, at high $\mathcal{M}$ the differences compared to the $T = \text{constant}$ assumption of Eq. (13) are modest, since $\mathcal{M}_l^{-2}$ falls off steeply away for $l > l_{\text{sonic}}$.

3.5 Choices made and other possibilities

We have endeavored through the previous sections to formulate a model with as few parameters as possible, based on simple physical considerations. Indeed, Eq. (13) involves just two physically motivated free parameters, κ and ξ, to describe the variation in a function, $\mathcal{P}_l(\ln \rho)$, across all scales in the system, for a wide range of turbulent Mach numbers. We shall see below (Sec. 4) that the model works relatively well in comparison to numerical simulations, both for measures that consider the variation in global parameters with physical parameters (e.g., the variance–Mach-number relation) and for measures in individual simulations (e.g., power spectra and the density PDF).

However, we feel it useful to reiterate the choices that have been made throughout the derivation, since some of these can be evaluated directly from simulation (or perhaps observational data). In this way, one might imagine calibrating certain aspects of the model, for example, to improve the accuracy of star-formation models. Given the success of the general shape of the PDF (H13), here we consider various aspects of the model that might be modified (and the possible utility in doing so), while retaining the compound-log-Poisson structure.

The single-step PDF The choice of an exponential PDF for the size of a single jump $\mathcal{P}_\delta$ (Fig. 2) was in part arbitrary, for the sake of convenience. For example, a similar $\mathcal{P}_\lambda$ is obtained with a δ function (this is used in most subsonic intermittency models; She & Leveque 1994; Boldyrev 2002; Hopkins 2015b; Mallet & Schekochihin 2017), or with a shifted Gamma distribution. There are, however, some important properties, which, if not satisfied would cause $\mathcal{P}_l(\ln \rho)$ to look quite different. In particular, the presence of an absolute maximum for $\delta \ln \rho$ is important, since without this $\mathcal{P}_l(\ln \rho)$ extends to infinitely high densities. Further, if this maximum is not equal to ϵ, the value of $\delta \ln \rho$ when there is no event, one has a similar problem, since as $\Gamma \to 1$ there is a nonzero probability of an arbitrarily large number of events n.

Number of structures encountered The proportionality between the probability of an event a and the jump size in scale $\delta r = \ln \Gamma$ is an important parameter that controls the level of intermittency for a given variance (i.e., the relation between $S_{\ln \rho}$ and T). In our model this is set by relating a to ϵ using $\langle \rho \rangle = 1$, then setting ϵ to the maximum possible density possible from a volume change in ξ dimensions $\epsilon = \xi \delta r$. While the proportionality between ϵ and δr simply relies on having a density field that is approximately scale invariant, the value for ξ is less well constrained. It is reasonable to expect $\xi < 3$, although its exact value depends on properties of the density field such as the density in "unshocked" regions. We have found empirically that $\xi \approx 1.3 \to 1.5$ gives a more accurate match to data (the exact value is hard to constrain given the significant scatter seen in numerical results; see Fig. 4), which is presumably related to the maximum density being closer to L/l as opposed to $(L/l)^3$ since compression happens primarily along one dimension (in other words, the maximum possible density is when all of the mass is contained within a single 2-D shock).

Variation of T with scale The variation in T with scale, and/or with Mach number, is difficult to constrain precisely, primarily because the system is *not* scale invariant at moderate Mach number. Specifically, although the sonic scale l_{sonic} is the only physically important scale above the viscous scale (which is ideally well into the subsonic regime), and so shock widths should eventually scale with l_{sonic}, it is hard to know how far above l_{sonic} it is necessary to go before this occurs. This implies that the shock width could deviate from $\sim \kappa \mathcal{M}^{-2}$; in other words, κ could depend on $\mathcal{M}$ at moderate $\mathcal{M}$. Nonetheless, the general form of T—an increase at low $\mathcal{M}$, followed by a flattening at high $\mathcal{M}$—is quite robust. Based on fits to numerical simulations and power spectra (see Secs. 4.1 and 4.4), we have found that the form (12) slightly underpredicts the increase in T with $\mathcal{M}$; i.e., it should asymptote more slowly to $T = \text{const.}$. Physically, this implies that the fraction of the mass contained in individual shocks should increase with $\mathcal{M}$ at higher values of $\mathcal{M}$ than suggested by $r_{\text{shock}} = \kappa l_{\text{sonic}}$.
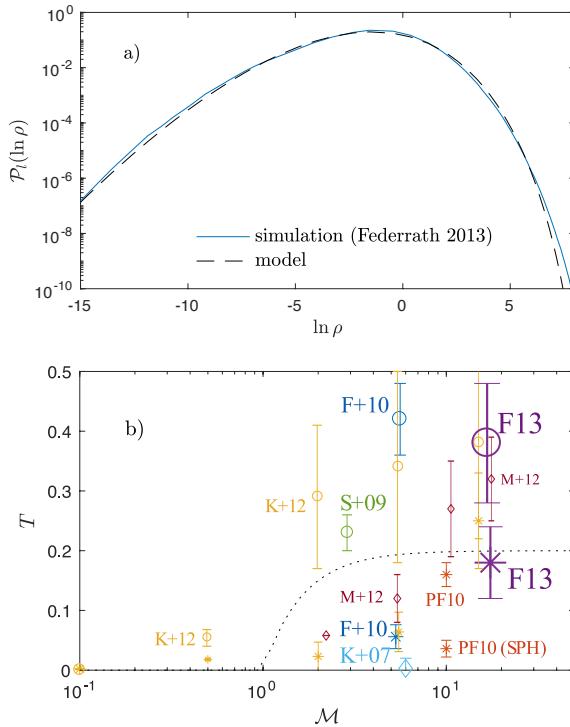
Another possible uncertainly stems from our assumption that the velocity scales as $v_l/c_s \sim \mathcal{M}(l/L)^\zeta$ with $\zeta = 1/2$, and that shocks are 2-D structures. If these parameters differ from these fiducial values (as may be the case; see, for example Federrath et al. 2008; Federrath 2013), this will also change the variation of T with $\mathcal{M}$. The sign of the change is such that an increase in shock dimension,[5] or an increase in ζ, causes T to increase with $\mathcal{M}$ (i.e., T changes from being constant at $\mathcal{M} \gg 1$ to being a slowly increasing function of $\mathcal{M}$, although it must eventually flatten out).

Finally, it worth emphasizing why it can be hard to describe the full density statistics with two parameters. The primary difficulty is that, unlike models that assume log-normal statistics, the density variance and its variation with scale are now entangled with the distribution's intermittency. For example, the prediction for the density-variance–Mach number relation depends strongly on T (or κ) and its variation with $\mathcal{M}$. Thus, any attempt to increase the variance by increasing κ creates unphysically intermittent density distributions. One can partially compensate for this by modifying ξ, higher values of which will increase the variance without much changing the intermittency, but this only works to some degree. Further, it is then necessary to match any measurements to different simulations across a variety of Mach numbers. In this regard, similar models for subsonic turbulence (e.g., She & Leveque 1994) are more easily constrained: there are more known parameters (e.g., the power spectrum), and any model is required to fit only one simulation (there is an inertial range, so there is no requirement for a model that remains accurate across all Mach numbers). In the tests of the following section, we compare directly to data from numerical simulations. The most stringent of these tests is the explicit calculation of $\mathcal{P}_l(\ln \rho)$ in Sec. 4.3, which probes the variation in both density variance and intermittency with scale.

4 PREDICTIONS AND NUMERICAL COMPARISONS

In this section, we outline the main predictions of the model, comparing these to results from previous works and several numerical simulations. In addition to the basic functional form of the PDF, which is well-known to accurately match simulations (Hopkins 2013b; Federrath 2013; Konstandin et al. 2016), the model's scale

---

[5] This can take on noninteger values if the shocks have a fractal structure on scales $l \gg l_{\text{sonic}}$.

Figure 3. (a) Comparison of the model (dashed black line) to the volume-weighted density PDF from the highest resolution simulation currently available, that of Federrath (2013) at 4096^3. The simulation uses solenoidal forcing and has a Mach number of 17.4 ± 1.1, and the fit shown has parameters $\kappa = 0.24$, $\xi = 1.5$ [this corresponds to $T = 0.2$, $S = 4.1$ using Eq. (14)]. Federrath (2013) also presents a compressibly forced simulation at similar Mach number, which causes a density PDF of much higher intermittency $T \approx 0.4$ and is also fit very well by model (see Federrath 2013 Fig. 4). (b) Measurements of T taken from a variety of simulations as a function of Mach number. Circle markers indicate simulations with compressive forcing, asterisks indicate solenoidal forcing, and diamond markers indicate forcing that involves some mix of compressive and solenoidal modes. Marker sizes are scaled by simulation resolution (a simulation at N^3 has a marker size $\propto \sqrt{N}$) so as to emphasize the most significant data points. In addition to the 4096^3 simulations of Federrath (2013) (purple, labelled F13), this data is taken from H13 based on Federrath et al. (2010) (blue, labelled F+10, 1024^3), Price & Federrath (2010) (red PF10, 512^3; SPH refers to their smoothed-particle hydrodynamics simulation), Konstandin et al. (2012) (yellow K+12, 512^3), Schmidt et al. (2009) (green S+09, 768^3), Kritsuk et al. (2007) (light blue K+07, 1024^3), Molina et al. (2012) (maroon M+12, 256^3). H13 lists the relevant parameters for each simulation in Table 1 (see also H13 Fig. 3). The dotted line shows the function $T = \kappa(1 - \mathcal{M}^{-2})$ for $\kappa = 0.2$, which was proposed in Sec. 3 based on the physical size and density contrast of shocks. Note that compressible forcing leads to higher intermittencies (T). With the large scatter in the data, it is unclear whether the simple model for T proposed in Sec. 3.3 is correct, but there does not appear to be a strong further increase in T with $\mathcal{M}$ for $\mathcal{M} \gtrsim 7$ (see Sec. 3.5).

dependence implies we can predict measures of the statistical variation with scale, such as power spectra and structure functions. Each of these is agrees within uncertainty to results from numerical simulations. In addition, in App. B we test the shock-width hypothesis $r_{\text{shock}} \sim \kappa l_{\text{sonic}}$, to check basic consistency with the model for T laid out in Sec. 3.3.

4.1 Density PDF: basic form

The shape of the density PDF is shown for illustration purposes in Fig. 3(a), which compares the form (5) to the numerically measured density PDF from the highest-resolution isothermal supersonic turbulence simulation yet run, from Federrath (2013). As also shown in Hopkins (2013b) for a range of other simulations, the quality of the agreement with the numerical PDF is impressive, with close-to-perfect agreement seen far into the tails of the distribution where the deviation from log normality is very significant.

The variation of the intermittency parameter T with Mach number is the first prediction of the model beyond Hopkins (2013b). In particular, we predict that T should be approximately constant with $\mathcal{M}$ for $\mathcal{M} \gg 1$, but may depend on the degree of compressibility (i.e., the ratio of solenoidal to compressive motions) of the turbulence, because this will change the shock density contrast b and/or shock width (compared to l_{sonic}). As shown in Fig. 3(b), these behaviors are indeed observed in simulation data (insofar as the very large uncertainties permit). In particular, T is very small for $\mathcal{M} < 1$, rises rapidly to $\mathcal{M} \sim 3 \to 5$, then appears to stay constant between 0.15 and 0.4 above this (possibly with some slow increase with $\mathcal{M}$, more simulations are needed to address this more accurately). In addition, the 4096^3 simulations of Federrath (2013) show a large difference in T between solenoidally and compressively forced simulations ($T \approx 0.2$ and $T \approx 0.4$ respectively) as expected from the arguments in Sec. 3.3.

It is worth noting that the intermittency (T) measured from simulations can vary significantly with numerical resolution and the numerical method. For example, Fig. 5 of Federrath (2013) illustrates how under-resolved simulations can overestimate T, while the Price & Federrath 2010 SPH simulations and Kritsuk et al. (2007) adaptive-mesh-refinement simulations produce very low intermittencies [see Fig. 3(b), points PF10 (SPF) and K+07].

4.2 Density variance-Mach number relation

The density variance-Mach number relation is the simplest prediction of the model that depends on the variation of the PDF with scale (since higher Mach numbers have a larger range of scales $l \gtrsim l_{\text{sonic}}$). Phenomenological arguments and simulations in previous literature suggest that this relation is
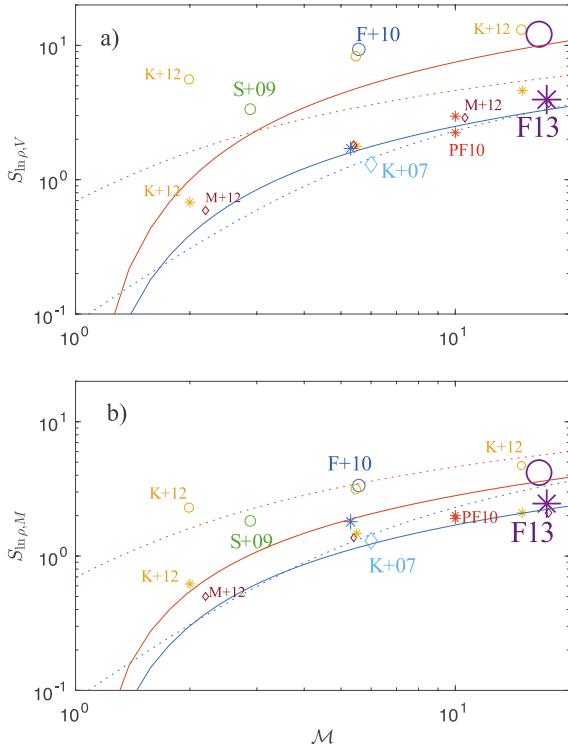
$$S_{\ln \rho} \approx \ln(1 + b^2 \mathcal{M}^2), \quad (15)$$

with $b \approx 0.3$ solenoidally forced turbulence, or $b \approx 1$ for compressively forced turbulence (see, for example, Padoan et al. 1997; Passot & Vázquez-Semadeni 1998; Lemaster & Stone 2008; Price et al. 2011; Molina et al. 2012). This "standard" result does not include a distinction between the volume-weighted variance $S_{\ln \rho, V}$ and the mass-weighted variance $S_{\ln \rho, M}$, since these are identical when the density is distributed log-normally.

From Eq. (13) and $S_{\ln \rho, V} = 2T^2 \lambda$, it is clear that since $\lambda \propto \ln(L/l)$, the model predicts $S_{\ln \rho} \propto \ln(\mathcal{M}^2)$ for $\mathcal{M} \gg 1$ (i.e., once $T \sim$ const.). This is a generic consequence of the constant accumulation of variance as a function of scale in log space, so this form is shared between any compound-log-Poisson model with scale-independent parameters. More precisely, the "exact" result, using T from Eq. (12) and Eq. (14), is

$$S_{\ln \rho, V} = 2\xi \kappa(\kappa + 1)\ln(\mathcal{M}^2) + \kappa \xi(1 - \mathcal{M}^{-2})[2 + \kappa(3 - \mathcal{M}^{-2})], \quad (16)$$

which becomes $S_{\ln \rho, V} \approx 2\xi \kappa(1 + \kappa)\ln(\mathcal{M}^2)$ for $\mathcal{M} \gg 1$. While this form is not identical to $S_{\ln \rho} \approx \ln(1 + b^2 \mathcal{M}^2)$, it can be very similar for $\mathcal{M} \gtrsim 5$ depending on the constant of proportionality. The

Figure 4. Density variance-Mach number relation (for $\mathcal{M} > 1$) as predicted by the model (solid lines) and as measured from simulations in previous literature (markers). Panel (a) shows the volume-weighted variance $S_{\ln \rho, V}$, while panel (b) shows the mass-weighted variance $S_{\ln \rho, M}$. We show model predictions for $\xi = 1.5$ and $\kappa = 0.2$ (blue, lower curve) or $\kappa = 0.6$ (red, upper curve) to indicate a range of values that might apply to solenoidal and compressively forced turbulence. The dotted curves show the standard result $S_{\ln \rho} \approx \ln(1 + b^2 \mathcal{M}^2)$ (Padoan et al. 1997) for $b = 0.3$ (blue) and $b = 1$ (red), respectively for solenoidal and compressive forcing (Federrath et al. 2010). Note that for the standard result, the volume-weighted and mass-weighted variances are the same since the PDF is assumed to be log-normal. The simulation results are as listed in Fig. 3(b) (see H13), with the marker size again scaled by simulation resolution. Although there is a large amount of scatter in the simulation results, the proposed model fits the data at least as well as the standard fit and captures the difference between the volume- and mass-weighted distributions.

question then becomes: For a reasonable intermittency (i.e., a value of T that matches that measured from the PDF), does the model prediction $S_{\ln \rho, V} \approx 2\xi\kappa(1+\kappa)\ln\mathcal{M}^2$ [or Eq. (16)] also match the measured $S_{\ln \rho, V}$?

In Fig. 4, we compare the model prediction with the standard result $S_{\ln \rho} \approx \ln(1 + b^2 \mathcal{M}^2)$ and various previous simulation results for $\mathcal{M} > 1$. This is done for both the volume-weighted variance [Fig. 4(a)] and the mass-weighted variance [Fig. 4(b)]. We plot $S_{\ln \rho}$ in each case for the model parameters $\kappa = 0.2$ and $\kappa = 0.5$, which are chosen to illustrate a range of intermittencies seen in solenoidally and compressibly forced simulations.[6] Given the significant scatter, the agreement of the model prediction is decent for these reasonable values of κ, and it seems fair to say that the model

---

[6] The values of T_l from Eq. (14) are somewhat lower than κ. For example, $\kappa = 0.5$ gives an intermittency parameter $T \approx 0.4$ for the compressible simulation of Federrath (2013), which is close to the measured value.

relation is of (at least) a similar quality to the standard result. Both results appear to somewhat underestimate the compressible variance, although more simulations at higher resolution are needed to better assess the trends at higher Mach number. We also see better agreement between the predicted and measured mass-weighted variances $S_{\ln \rho, M} = (1+T)^{-3} S_{\ln \rho, V}$, compared to the standard result. This is unsurprising since the effects of intermittency generically act to reduce $S_{\ln \rho, M}$ compared to $S_{\ln \rho, V}$. It is also worth reiterating that the model neglects the subsonic contribution to the variance, which is significant for simulations with $\mathcal{M}$ approaching 1, and is the cause of the variance under-prediction at low $\mathcal{M}$.
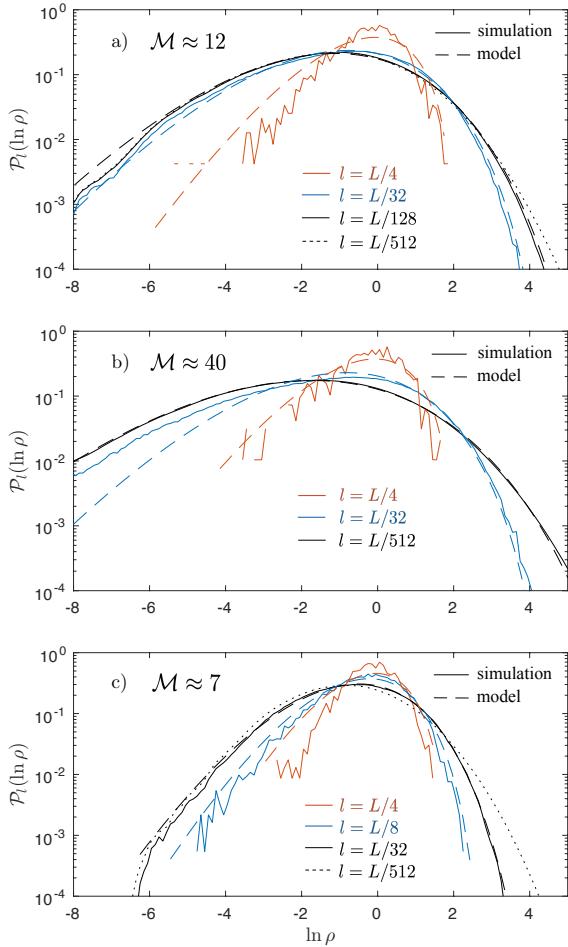
4.3 Density PDF as a function of scale

A more stringent test of model predictions is to compute $\mathcal{P}_l(\ln \rho)$ directly from simulation, viz., bin the density into volumes of size l^3 then compute the density PDF. Unfortunately, so far as we are aware there is no measurement of this in previous literature, despite its physical, as well as theoretical, relevance. We have thus run a variety of isothermal turbulence simulations to make such measurements directly. These simulations use the GIZMO code (Hopkins 2015a; Hopkins & Raives 2016) with the Meshless-Finite-Mass (MFM) method and 256^3 elements. Although this resolution may be relatively low by modern standards, the Lagrangian nature of the MFM method more accurately captures the high density shock regions by naturally having higher resolution in such regions (Price & Federrath 2010), and the MFM method has proven very accurate in a wide variety of test problems (Hopkins 2015a; Hopkins & Raives 2016). That said, given the significant dependence of intermittency properties on resolution and numerical method (Price & Federrath 2010; Federrath 2013), it will be important to verify the scaling of these results with resolution. The simulations are forced by a Ornstein-Uhlenbeck process with an equal mix of solenoidal and compressive large-scale modes, as described in (Bauer & Springel 2012). Different forcing strengths are used to drive turbulence across a range of Mach numbers. PDFs are calculated by depositing the density field onto a 512^3 uniform grid using a Gaussian kernel for each Lagrangian mesh element (of width $\sigma = \sqrt{3/40}h$, where h is the cell smoothing length; Dehnen & Aly 2012; Hopkins 2015a), then averaging over successively larger volumes to form the PDF as a function of scale. This grid-based method agrees with the volume-weighted PDF calculated directly from the Lagrangian mesh for the finest $N = 512$ grid.[7]

Figure 5 compares results from simulations at (a) $\mathcal{M} \approx 12$, (b) $\mathcal{M} \approx 40$, and (c) $\mathcal{M} \approx 7$ with model predictions (shown with dashed lines). In each case, to specify the model, we use the measured $\mathcal{M}$, $\xi = 1.3$, and choose κ to match the variance on the smallest supersonic scales.[8] We then compare the model predic-

---

[7] There is some discrepancy at the lowest densities. This is expected because the density field deposited using the Gaussian kernel contains regions of lower density (the regions in between mesh elements) than that of the lowest density mesh elements. To find the true density in such regions one should use the "gather" method for constructing gridded data, as this is actually used in the simulation (Hopkins 2015a); however the Gaussian kernel method we use probably provides a better representation of the true field than the PDF from Lagrangian data, which is effectively under-sampling the lowest density regions.

[8] This value of $\xi = 1.3$ works slightly better for these simulations than the $\xi = 1.5$ plotted in Fig. 4. Given the large scatter across different simulations and numerical methods, it is not surprising that model parameters should need to be modified slightly to fit a particular simulation set.

Figure 5. Density PDF $\mathcal{P}_l(\ln\rho)$ for (a) $\mathcal{M}\approx 12$, (b) $\mathcal{M}\approx 40$, and (c) $\mathcal{M}\approx 7$ turbulence. In each panel, solid curves show the measured PDFs of the density averaged over a variety of scales, while dashed curves show model predictions for the same parameters. In each case, we only compare the model with simulations on scales $l > l_{\rm sonic} \approx \mathcal{M}^{-2}$; specifically for (a) $\mathcal{M}\approx 12$ with $l_{\rm sonic} \approx L/150$, we take $l = L/128$ (black, widest curve), $l = L/32$ (blue, middle curve), and $l = L/4$ (red, narrowest curve); for (b) $\mathcal{M}\approx 40$ with $l_{\rm sonic} \approx L/1600$, we take $l = L/512$ (black), $l = L/32$ (blue), and $l = L/4$ (red); and for (c) $\mathcal{M}\approx 7$ with $l_{\rm sonic} \approx L/50$, we take $l = L/32$ (black), $l = L/8$ (blue), and $l = L/4$ (red). In this way the subsonic contributions to the variance, which are not included in the model, are explicitly removed from the simulation results. We take $\kappa = 0.24$ (a-b) and $\kappa = 0.18$ (c), with $\xi = 1.3$ in all cases, illustrating its success across a range of $\mathcal{M}$ with little change to κ (see text for discussion). In each panel, we also show the PDF on the smallest scales measured, $l = L/512$, and the difference between this and the solid black curve explicitly illustrates the contributions from subsonic scales in (a) and (c). Although there seems to be a slight under-prediction of the intermittency on the largest scales $l = L/4$, the numerical PDF is likely also affected by discretization and insufficient statistics, which would tend to raise the low-density tail.

tions for the intermittency and variance on scales $l > l_{\rm sonic}$ with that measured by binning the density on the same scale (for three values of l). More precisely, in the $\mathcal{M}\approx 12$ simulation [Fig. 5(a)], $l_{\rm sonic} \approx L/150$, so we compare data on scales $l = L/128$, $l = L/32$, and $l = L/4$; in the $\mathcal{M}\approx 40$ simulation [Fig. 5(b)], $l_{\rm sonic} \approx L/1600$, so we compare data on scales $l = L/512$, $l = L/32$, and $l = L/4$; and in the $\mathcal{M}\approx 7$ simulation [Fig. 5(c)], $l_{\rm sonic} \approx L/50$, so we compare data on scales $l = L/32$, $l = L/8$, and $l = L/4$. This method is chosen

to explicitly remove the subsonic scales from the comparison, since these are not included in the model.

The agreement of the model to simulation is seen to be relatively good. In particular, identical model parameters ($\kappa = 0.24$ and the measured $\mathcal{M}$) give very good fits to $\mathcal{M}\approx 12$ and $\mathcal{M}\approx 40$ across a wide range of scales in the system. A similar, though slightly lower, value of κ ($\kappa = 0.18$) gives a very good fit at lower $\mathcal{M}\approx 7$. We attribute this difference in κ to the slight underestimation of the increase in T with $\mathcal{M}$ in the model [Eq. (12)]. Although the model possibly overpredicts the variance at the largest scale ($l = L/4$) in each case, it is worth noting that this scale is very close to the driving (at $\sim L/2$) and may be influenced by this. Further, the statistics at $l = L/4$ in each case are somewhat undersampled (there are only 64 values per density snapshot), and more values would tend to increase the low density tail.

Finally, it is worth briefly mentioning the contribution of the subsonic scales to the full 512^3 density PDF (dotted line in each panel of Fig. 5). As can be seen from Fig. 5(a) and (c), the subsonic scales have the effect of decreasing the intermittency (i.e., making the distribution more log-normal) by contributing to the high-density tail. This should be expected, since the subsonic contribution will involve large numbers of small events (i.e., small T). While the effect appears more significant in the $\mathcal{M}\approx 7$ simulation (compared to the larger $\mathcal{M}$ cases), in fact, the absolute increase in the density maximum—i.e., the difference between $\rho_{\rm max}$ with and without the subsonic contributions— is about the same at $\mathcal{M}\approx 7$ and $\mathcal{M}\approx 12$. It appears larger at $\mathcal{M}\approx 7$ due to the smaller contribution to the variance from supersonic motions. This justifies our neglect of subsonic scales in the model, which is primarily intended for study of the $\mathcal{M}\gg 1$ limit. Since the subsonic contribution occurs on the very smallest scales of any simulation, and will thus presumably be affected by the numerical method, it is possible that they play a role in the wide scatter seen between different simulations in both the density variance-Mach number relation and the intermittency (see Figs. 4 and 3). See Federrath et al. (2010) for further discussion.

4.4 Spectrum

As shown in App. A, the density power spectrum $\phi_\rho(k)$ is related to the variation in the second order statistics (variance and mean) of the PDF with scale. In particular, for some variable s, the 1-D power spectrum is

$$\phi_s(k) \sim \frac{d}{dk}(S_l + \bar{s}_l^2),\qquad(17)$$

where S_l and $\bar{s}_l^2$ are the variance and mean of $\mathcal{P}_l(s)$. From Eq. (5), the volume-weighted variance of ρ can be calculated as (H13),

$$S_\rho = \exp\left(\frac{S_{\ln\rho}}{(2T+1)(T+1)}\right) - 1.\qquad(18)$$

Then, using $\langle\rho\rangle = 1$, the simplified form for S, $S_{\ln\rho} = 2\xi T(1+T)\ln(L/l)$ (i.e., neglecting the scale variation of T),[9] and approximating $T \approx \kappa$ for $\mathcal{M}\gg 1$, one obtains the scaling

$$S_{\rho,l} + \bar{\rho}_l^2 \sim \left(\frac{l}{L}\right)^{-\frac{2\xi\kappa}{2\kappa+1}}.\qquad(19)$$

---

[9] The power spectrum can be derived analytically using the full integrals, Eq. (14); however the resulting expressions are very complicated and no longer follow a power law at high k.

The model thus predicts the ρ power spectrum

$$\phi_\rho(k) \sim k^{-\nu} \quad \nu = \frac{1+2\kappa(1-\xi)}{1+2\kappa}, \qquad (20)$$

in the limit $\mathcal{M} \gg 1$ for $1/k \gg l_{\text{sonic}}$. This spectrum is somewhat less steep than k^{-1} (it is k^{-1} $\kappa \to 0$ or $\xi \to 0$) and becomes less steep with increasing κ or ξ—for example, the parameters used in Fig. 5 give $\phi_\rho(k) \sim k^{-0.56}$. The same procedure for the power spectrum of $\ln \rho$, using $\langle \ln \rho \rangle = -S_{\ln \rho}(1+T)^{-1}/2$ leads to

$$\phi_{\ln \rho}(k) \sim \frac{2\xi\kappa}{9}\left(k^{-1} + \frac{3\ln k}{k}\right) + \mathcal{O}(\kappa)^2, \qquad (21)$$

implying the power spectrum of $\ln \rho$ is not expected to be a power law but is close to $\sim k^{-1}$.

An important difference compared to previous models of the supersonic density power spectrum (Saichev & Woyczynski 1996; Kim & Ryu 2005; Konstandin et al. 2016) is that we do not predict a density spectrum that approaches k^0 for $\mathcal{M} \gg 1$. Instead, our prediction is that the spectrum approaches some power law between k^0 and k^{-1} that depends relatively strongly on the intermittency of the density distribution (through κ). We thus predict a steeper spectrum for solenoidal compared to compressive forcing (since measured values of T are larger for compressive forcing); e.g., using the values $\kappa \approx 0.2$ and $\kappa \approx 0.5$ (with $\xi = 1.3$) suggests the spectra $\sim k^{-0.63}$ and $\sim k^{-0.35}$ for solenoidal and compressive forcing respectively. We also predict that the $\ln \rho$ spectrum should not depend on the forcing so strongly, although it is also not a power law. These predictions are valid only for scales well above the sonic scale, since model parameters change significantly as $\mathcal{M}_l \to 1$.

With currently available simulation data, these predictions are difficult to verify or disprove. While a number of studies have considered density power spectra across a range of $\mathcal{M}$ (Kim & Ryu 2005; Kritsuk et al. 2007; Kowal et al. 2007; Konstandin et al. 2016), the scaling exponent depends significantly on resolution (see Konstandin et al. 2016, Fig. 8). Nonetheless, the predicted density spectrum scaling does not appear to disagree with previous results, although the spectrum is likely somewhat steeper than predicted at modest $\mathcal{M}$. This is expected because the additional decrease in T with scale at moderate $\mathcal{M}$ [see Eq. (12)] is not taken into account in Eq. (20) and acts to steepen the spectrum. Similarly, the simulations presented in Fig. 5 have density power spectra consistent with predictions at high $\mathcal{M}$ ($\sim k^{-0.6}$ at $\mathcal{M} \approx 40$ and $\sim k^{-0.7}$ at $\mathcal{M} \approx 12$; comparable to the prediction $\kappa = 0.24$, $\sim k^{-0.56}$) but are a little steeper at $\mathcal{M} \approx 7$ ($\sim k^{-0.9}$), presumably due to the scale dependence of T.

The results for the spectrum of $\ln \rho$ are even less well known, to our knowledge appearing in previous literature only in Kowal et al. (2007) (for magnetohydrodynamic turbulence) and Federrath et al. (2010). Federrath et al. (2010) reports $\ln \rho$ spectra of $\sim k^{-1.6}$ and $\sim k^{-2.3}$ for solenoidal and compressible turbulence respectively at $\mathcal{M} \approx 5.5$, while Kowal et al. (2007) report $\sim k^{-1.5}$ for $\mathcal{M} \approx 7$ (or perhaps flatter at the largest scales); however, because these simulations each have a relatively modest Mach number, a spectrum steeper than k^{-1} should be expected since they are in the regime where T increases with l/L [i.e., before the plateau in Fig. 3(b)], which means the accumulation of variance with $\ln(l)$ is faster than linear. Our simulations give somewhat unclear results, although also appear to show steeper spectra than predicted (somewhere between k^{-1} and k^{-2} for the largest scales).

Overall, these results may suggest that the $T(\mathcal{M})$ scaling $T \sim \kappa(1-\mathcal{M}_l^{-2})$ [Eq. (12)] underestimates the true increase of T with $\mathcal{M}$ somewhat (see Sec. 3.5). For the sake of example, if we assumed a different model with a faster increase in T, $\kappa \sim \mathcal{M}_l^2 \sim (l/L)\mathcal{M}^2$ at moderate $\mathcal{M}$, this would steepen the $\ln \rho$ power law to $\sim k^{-2}$, and the power law of ρ by a factor $\sim k^{-1}$. Study of higher resolution simulations at higher $\mathcal{M}$ (for example, the simulations of Federrath 2013) is required to better assess our predictions. Nonetheless, the general arguments presented here should provide a useful framework for interpreting results.

5 EXTENSIONS

Given the simple relation between the intermittency parameter T and the physical properties of shocks, it is possible to straightforwardly extend the model to situations with more complex physics. Here, we briefly consider turbulence with a non-isothermal polytropic equation of state, as relevant for various phases of the ISM (see, for example, Audit & Hennebelle 2005; Gazol & Kim 2013; Federrath & Banerjee 2015 and references therein). Other extensions—e.g., to supersonic magnetohydrodynamic (MHD) turbulence—are also possible using similar ideas. Note that the discussion and results in this section are intended to be of a qualitative nature. While the simple extensions we propose do give a reasonable match to simulation results, the purpose of the analysis is as much to illustrate the applicability of the shock model in Sec. 3, as to provide useful models for turbulent PDFs. With this in mind, some of the ideas discussed can likely be applied more rigorously if so desired; for example, to derive scalings for the low or high density tails of the PDF .

The key idea of the method—which is effectively that proposed in Passot & Vázquez-Semadeni (1998) extended to non-lognormal isothermal PDFs—is to assume that the primary effect of the non-isothermal equation of state is to modify the sound speed with the density. This in turn modifies the local Mach number and causes the shock density contrast to depend on the local value of the density. As shown in Federrath & Banerjee (2015), this behavior is indeed seen as a correlation between ρ and $\mathcal{M}$ in the turbulent joint Mach number-density PDF, as well as leading to a useful estimate for the modified density variance-Mach number relation when applied to the shock-jump condition.

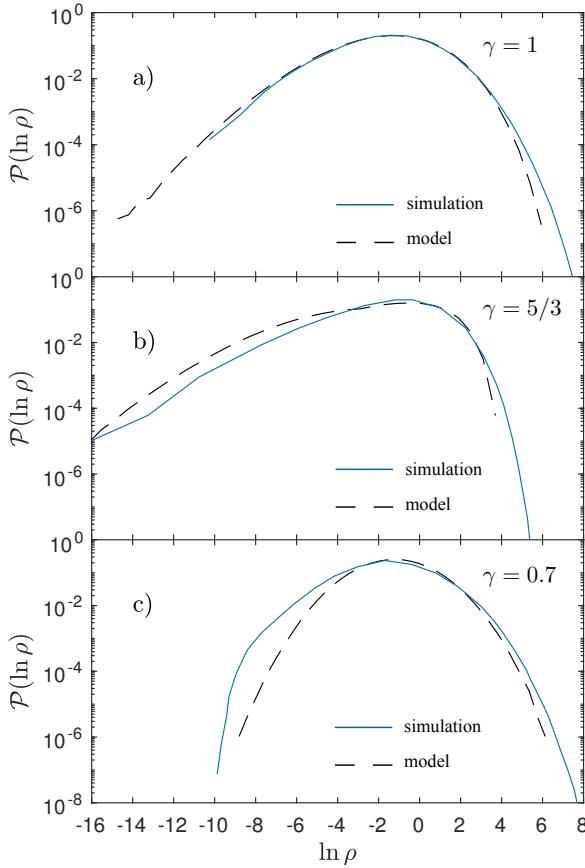More precisely, for a polytropic equation of state $p/p_0 = (\rho/\rho_0)^\gamma$ (p is the pressure), one takes

$$\mathcal{M} \propto c_s^{-1} \sim \left(\frac{p}{\rho}\right)^{-1/2} \sim \rho^{(1-\gamma)/2} = \exp\left(\frac{1-\gamma}{2}\ln \rho\right), \qquad (22)$$

which is then used in the shock-density-contrast relation $(\rho_1/\rho_0) \sim b^2\mathcal{M}^2$. We thus see that with $\gamma < 1$, the system will have higher contrast shocks (compared to isothermal expectations) at high densities and lower contrast shocks at low densities, while $\gamma > 1$ leads to the opposite behavior. Within our model, this causes the mean jump size $\langle \delta \ln \rho \rangle - \epsilon = T$ to depend on the local value of the density through the replacement of $\mathcal{M}_l$ with $\mathcal{M}_l \exp[(1-\gamma)/2 \ln \rho]$, or

$$T \sim \kappa\left(1 - \frac{L}{l}\mathcal{M}^{-2}e^{(\gamma-1)\ln \rho}\right), \qquad (23)$$

(with $T = 0$ if $\mathcal{M}_l^{-2}e^{(\gamma-1)\ln \rho} > 1$).[10] It is clear that this form of T will decrease the low-density tail for $\gamma < 1$ due to the fast increase in

---

[10] Note that we have neglected a potentially important effect here, which is the change in shock contrast and width with γ due to the differing sound speeds on either side of the shock. The density contrast is derived in the form of a transcendental equation in Federrath & Banerjee (2015); however, the complexity of these expressions, as well as the necessity of deriving

Figure 6. Predicted density PDF for non-isothermal polytropic turbulence (dashed black line) compared to the simulations of Federrath & Banerjee (2015) (solid blue line). The Mach numbers are $\mathcal{M} = 11.6$ ($\gamma = 1$), $\mathcal{M} = 13.3$ ($\gamma = 5/3$), and $\mathcal{M} = 8.4$ ($\gamma = 0.7$), and the Federrath & Banerjee (2015) simulations were run at resolutions of 2048^3 ($\gamma = 5/3$ and 0.7) or 1024^3 ($\gamma = 1$). For the model, there are *no* free parameters used to fit the non-isothermal PDFs: we use the same value of $\kappa = 0.26$ in each case (this was chosen to match the $\gamma = 1$ distribution) and the physical value of the Mach number listed above. Although the fits here are not perfect, the method does a good job at capturing the qualitative change in the PDF shape considering there are no free parameters. In addition, the low density regions where the largest discrepancies are seen have more significant numerical error bars and resolution dependence (see Federrath & Banerjee 2015 Fig. 4), and there is presumably some contribution to the high densities from the subsonic scales (see, e.g., Fig. 5(a)).

$e^{(\gamma - 1)\ln \rho}$. In contrast, for $\gamma > 1$ the low-density tail will increase in probability, because the cascade can proceed further (go to smaller scales) before $T \to 0$, meaning individual $\delta \ln \rho$ jumps are larger.

Results are illustrated in Fig. 6, which shows the comparison

the density jump based on the shock width (which also must scale with the density), leads to complex systems of transcendental equations that are difficult to use in the model. The method is thus more similar to Passot & Vázquez-Semadeni (1998) as opposed to Federrath & Banerjee (2015). Although working this out correctly will certainly change the functional dependence of T on $\mathcal{M}$, as well as adding γ dependence into the shock jump size (κ or some similar parameter), the key differences compared to an isothermal equation of state—in particular the reduction in the size of jumps at low (high) density for $\gamma < 1$ ($\gamma > 1$)— are retained in the much simplified version.

of this model to the volume-weighted PDF data from Federrath & Banerjee (2015). Despite a variety of limitations (see below), we see that the qualitative trends for the PDFs are captured well. In particular, at $\gamma > 1$ we see a faster fall off at high densities and a long tail at low densities with a slope that generally matches the simulation PDF, while at $\gamma < 1$ the lower densities are significantly reduced (although the prediction is too severe, cutting off at somewhat higher densities than in the simulation). Given the possible resolution dependence of the low probability regions (see Federrath & Banerjee 2015 Fig. 4, second row), the overall agreement is encouraging.

To calculate the illustrated PDFs, we use a simple Monte-Carlo method with the prescription for T taken from Eq. (23), using the same value of $\kappa = 0.26$ and $\xi = 1.5$ in each case, with $\mathcal{M}$ as quoted in Federrath & Banerjee (2015). We thus have no free parameters to aid in the fitting for the nonisothermal PDFs in Fig. 6, and the fit could potentially be significantly improved by optimizing over κ. (Note that, based on physical arguments, κ *should* be modified somewhat with γ, becoming smaller with increasing γ due to the change in shock jump condition calculated in Federrath & Banerjee 2015.) For consistency with the simulations, we retain scales down to $L/l \sim 1024$ in the Monte-Carlo cascade (estimating twice the grid scale as the minimum resolvable scale). In addition, the subsonic scales are included in the illustrated PDFs making a direct comparison difficult, and at this Mach number $\mathcal{M} \sim 12$ these will have a minor but observable contribution to the high-density probability (e.g., compare the $L/l = 512$ and $L/l = 128$ curves in Fig. 5(a), which explicitly shows the subsonic contribution at a similar Mach number). It is interesting to note that the low-density tail of the $\gamma > 1$ PDF may flatten further with resolution beyond 2048^3 (this is seen in our model if a wider range of scales is kept): even at low velocities, very low density regions remain supersonic with strong shocks that cause large density contrasts (see also Federrath & Banerjee 2015 Fig. 4).

Finally, we note that similar ideas can be applied to MHD turbulence. A simple method, used in Padoan & Nordlund (2011); Molina et al. (2012); Federrath & Banerjee (2015) for the density variance-Mach number relation, is again to consider how the Mach number is altered by the influence of the magnetic field on the total pressure,

$$\mathcal{M} \sim c_s^{-1} \sim \frac{\rho}{p_{\text{gas}} + p_{\text{mag}}} \sim c_{s0}^{-1}(1 + \beta^{-1})^{-1/2}, \qquad (24)$$

where $\beta = p_{\text{gas}}/p_{\text{mag}}$ is the ratio of thermal to magnetic pressure and c_{s0} is the sound speed without the magnetic field. To apply this form of $\mathcal{M}$ to the density PDF model, we need a prescription for how B changes with ρ. While this remains uncertain, it unequivocally depends on turbulence parameters (e.g., Alfvén-Mach number and β; see Lithwick & Goldreich 2001; Cho & Lazarian 2003; Burkhart et al. 2009; Banerjee et al. 2009). As an example, taking $B \sim \rho^{1/2}$ (Crutcher 1999; Banerjee et al. 2009; Molina et al. 2012) we obtain a PDF of exactly the same functional form as the isothermal PDF, with shock sizes reduced by $1 + \beta^{-1}$ (this is effectively identical to the model of Molina et al. 2012). In contrast, a scaling $B \sim \rho^\chi$ with $\chi < 1/2$ acts to decrease the PDF at low densities, which is indeed seen in simulations (Molina et al. 2012). A similar effect would be seen if $B(\rho)$ became constant below some density threshold[11] (i.e., if the relation between B and ρ was not a power

---

[11] This form is suggested by the observations of Crutcher et al. (2010), who report a lower density bound below which the density and magnetic field are uncorrelated. It is also expected on physical grounds because the turbulence

law, but a more sudden change). An interesting consequence of this is that the increased log-normality observed in MHD turbulence is probably not due to increased Gaussianity in the underlying turbulence. Instead, we may be seeing suppression of the low-density tail of a compound-log-Poisson distribution, which causes the PDF to appear log-normal even though the underlying turbulence could have similar intermittency properties [this this is the same effect as in non-isothermal turbulence with $\gamma < 1$; see Fig. 6(c)]. While there are many interesting (and astrophysically relevant) issues to explore here, we postpone such studies to future work due to the uncertainties regarding the scaling of B with ρ.

6   DISCUSSION AND CONCLUSIONS

In this paper, we propose a simple phenomenological model to describe the distribution of density in supersonic turbulence. Given the turbulent Mach number $\mathcal{M}$ and two free parameters (κ and ξ) that relate to the physical properties of shocks, the model predicts the PDF of the density averaged over scale l, $\mathcal{P}_l(\ln \rho)$ [Eq. (13)]. Since $\mathcal{P}_l(\ln \rho)$ completely specifies the statistics of the density field, the model predicts all relevant statistic quantities of the density field: the density variance–Mach number relation, the density PDF and intermittency, power spectra, and structure functions. We see reasonable agreement between model predictions, results from previous literature, and our own set of simulations. The model is also straightforwardly extendable to more complex gas physics (e.g., varied gas equations of state, or magnetohydrodynamics) and shows decent agreement to recent simulations of nonisothermal turbulence (Federrath & Banerjee 2015).

The main predictions and results are summarized as follows:

• The gas density, averaged across scale l, is distributed according to the PDF suggested in H13; see Eq. (5). The intermittency parameter T controls the deviation from log-normality ($T = 0$ describes a log-normal distribution). This form of the PDF matches numerical measurements very well across many orders of magnitude (see Fig. 3). The intermittency and variance of the density PDF change with scale and Mach number.

• The density is arranged into a random collection of shocks across all scales (above the scale at which the velocity becomes subsonic). The physical size of the shocks and their relative density contrast are controlled by the model parameter $\kappa \sim r_{\rm shock}/l_{\rm sonic}$, which sets T in the density PDF. Larger and higher-density shocks create a density distribution that is more intermittent.

• Mathematically, the density is constructed via a compound-log-Poisson process. The size of each individual event (shock) is distributed according to an exponential distribution (see Fig. 2).

• The number of shocks encountered across some range in scales is set by the maximum density that is possible if the gas is compressed in ξ dimensions, where ξ is effectively a model parameter (its maximum is $\xi = 3$). Empirically, we find that $\xi \approx 1.3 \to 1.5$ gives a reasonable fit to data, but given the significant scatter in previous results and between numerical methods (see Fig. 4) the estimate is quite approximate.

• The parameter κ differs between compressibly and solenoidally forced turbulence, because the shocks are more intense with compressive forcing (Federrath 2013). Based on numerical PDFs (see also App. B for a more direct measurement)

κ ranges from ~ 0.2 to ~ 0.5 as the compressive fraction is increased (but could also be lower in some cases; see Pan et al. 2016).

• The density variance–Mach number relation is similar to the standard result $S_{\ln \rho} \approx \log(1 + b^2 \mathcal{M}^2)$ for values of κ that match the observed intermittency.

• The model predicts a density power spectrum for $\mathcal{M} \gg 1$ between $\sim k^{-1}$ and $\sim k^0$, depending on κ (and ξ) [see Eq. (20)], thus predicting a spectrum that is directly related to the intermittency. The power spectrum does not approach k^0 in the $\mathcal{M} \to \infty$ limit.

• We neglect the influence of subsonic motions on the density PDF, since these are negligible at high $\mathcal{M}$ and stem from different physical processes. However, subsonic contributions to the PDF can reduce the intermittency (see Fig. 5) and may be responsible for some of the scatter seen across numerical results (see Fig. 3).

• Extensions to the assumption of isothermal neutral gas may be included by considering the sound speed, and thus local shock size, to be a function of local gas density (as in Passot & Vázquez-Semadeni 1998). This leads to density PDFs that agree well with those observed in simulations with a nonisothermal equation of state (see Fig. 6).

More generally—particularly considering the very significant scatter between simulations reported in previous literature (see, e.g., Figs. 3 and 4)—the model can be seen as a framework for understanding density statistics and intermittency, describing how different statistical measures might be compared to provide interesting information about the underlying structures. This is particularly true in the moderate-$\mathcal{M}$ regime, which is most relevant physically and easiest to study numerically, but is not blessed with an true inertial range (due to the proximity of $l_{\rm sonic}$ to the scales of interest). For example, as mentioned throughout the text, our simple model for the shock size $r_{\rm shock} \sim \kappa l_{\rm sonic}$, probably underestimates the increase in T with $\mathcal{M}$, which could stem from the mass-fraction contained in shocks increasing somewhat from $\mathcal{M} \sim 1$ to $\mathcal{M} \gg 1$ (i.e., κ increasing with $\mathcal{M}$). In this vein, it is prudent to carry out further tests of the model using higher-resolution numerical simulations (ideally with differing numerical methods), in particular, direct measurements of $\mathcal{P}_l(\ln \rho)$ (as in Fig. 5) across a range of $\mathcal{M}$.

Of course, real turbulence in the ISM involves a wide variety of other physical effects, which could strongly modify the ideal isothermal behavior discussed through most of this work. For example, magnetic fields, self-gravity, dust, and more complicated radiation physics could all play key roles in some cases, and the ISM can hardly be considered a homogeneous medium. Given the physical motivations behind various choices in the model, some of these features can be included in extended versions of the model (see Sec. 5), albeit heuristically. Such extensions could be interesting to study in future work and potentially important for making astrophysically relevant predictions. The model could also form the basis for a description of other physical effects that are strongly influenced by turbulence. Star formation (Hopkins 2013a; Hennebelle & Chabrier 2013) is an obvious example for such applications, but there are also a variety other possibilities; for instance, the dynamics of dust grains, which are key in controlling the distribution of metals in the ISM (Draine 2003) and strongly affected by turbulence (Hopkins & Lee 2016; Lee et al. 2016).

will become Alfvénic in character ($v_A \propto B/\rho^{1/2} > v_l$) below some density (Lithwick & Goldreich 2001; Cho & Lazarian 2003).

APPENDIX A: DERIVATION OF THE DENSITY STRUCTURE FUNCTIONS AND POWER SPECTRA FROM $\mathcal{P}_L(\ln\rho)$

In this appendix we illustrate how to derive structure functions and power spectra from the scale variation variation of the PDF $\mathcal{P}_l(\ln\rho)$. This derivation is completely general and could apply to any statistical field for which one had $\mathcal{P}_l$.

Consider the variable s, denoting its average over scale l as s_l. We take s_l distributed according to the PDF $s_l \sim \mathcal{P}_l(s_l)$, with mean $\bar{s}_l = \int s_l \mathcal{P}_l(s_l)ds_l$ and variance $S_l = \int s_l^2 \mathcal{P}_l(s_l)ds_l - \bar{s}_l^2$. The first observation is that the isotropic autocorrelation of $s_{l'}$

$$R_{s_{l'}}(l) = R_{s_{l'}}(|l|) = \langle s_{l'}(x+l)s_{l'}(x)\rangle. \tag{A1}$$

is the same as $R_{s_{l''}}(l)$, so long as $l'' < l$ and $l' < l$. We also note that if $l' > l$,

$$R_{s_{l'}}(l) = S_l + \bar{s}_l^2, \tag{A2}$$

which follows because $s_{l'}$ is constant on scales less than l'. This implies

$$R_s(l) = S_l + \bar{s}_l^2, \tag{A3}$$

relating direct measurements of s to $\mathcal{P}_l$.

The second-order structure function is now easily calculated as

$$\langle \Delta s^2 \rangle = \langle [s(x+l)-s(x)]^2 \rangle = 2\langle s^2 \rangle - 2(S_l + \bar{s}_l^2). \tag{A4}$$

However, the nonlocality of Eq. (A4) (it depends on the smallest scales through $\langle s^2 \rangle$) is inconvenient, and it is more helpful to consider its derivative,

$$\frac{1}{2}\frac{d\langle \Delta s^2 \rangle}{dl} = -\frac{d}{dl}(S_l + s_l^2). \tag{A5}$$

Equation (A5) is more useful than Eq. (A4) because it lacks dependence on the smallest or largest scales in the system.

The 3-D power spectrum $\Phi_s(k)$ is related to the autocorrelation through the standard Fourier transform. However, since we are interested in the 1-D spectrum $4\pi k^2 \phi_s(k) = \Phi_s(k)$, the relation is instead (Davidson 2015)

$$R_s(l) = \int_0^\infty \phi_s(k)\mathrm{sinc}(kl)dk, \tag{A6}$$

where $\mathrm{sinc}(x) = x^{-1}\sin(x)$. Approximating $\mathrm{sinc}(kl) \approx \Pi(kl/2\pi)$, where $\Pi(x)$ is the tophat function (1 for $-1 < x < 1$, 0 otherwise), we see that the transform (A6) is related to a filtering operation
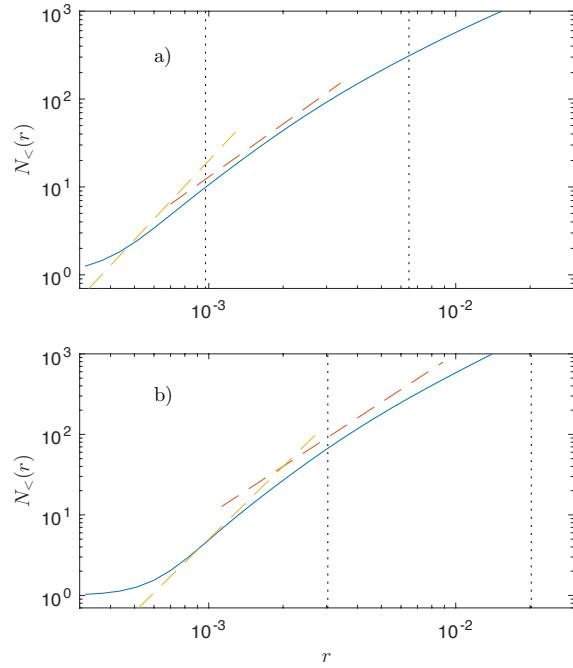
$$R_s(l) \approx \int_{2\pi/l}^\infty \phi_s(k)dk, \tag{A7}$$

or

$$\frac{d\langle \Delta s^2 \rangle}{dl} \approx \frac{2\pi}{l^2}\phi_s\left(\frac{2\pi}{l}\right). \tag{A8}$$

Neglecting numerical constants (we are only interested in the k-scaling of the power spectrum), we obtain

$$\phi_s(k) \sim \frac{d}{dk}(S_l + s_l^2), \tag{A9}$$

Figure B1. Average of $N_<(r)$ over snapshots and 10000 randomly chosen center cells for (a) $\mathcal{M} \approx 12$ and (b) $\mathcal{M} \approx 7$. The dashed red and yellow lines show r^2 and r^3 scalings respectively. The vertical dashed lines show the inferred sonic scale $l_{\rm sonic} \sim \mathcal{M}^{-2}$ (right) and $\kappa l_{\rm sonic}$ (left) with $\kappa = 0.15$. Although of narrow extent due to the flattening of $N_<(r)$ to $N_<(r) = 1$ for $r < r_{\rm cell}$, there is a region at r where the scaling is substantially steeper than r^2. The transition to $N_<(r) \sim r^2$ scaling occurs significantly below $l_{\rm sonic}$ but in rough agreement with $\kappa l_{\rm sonic}$ for both $\mathcal{M} \approx 12$ and $\mathcal{M} \approx 7$.

which fits with the intuition that the power spectrum should encode the change in the variance of s with scale.

APPENDIX B: SHOCK SIZES

In this appendix, we explicitly test the assumptions about shock width $r_{\rm shock}$ that went into deriving T. In particular, the scaling $r_{\rm shock} \sim \kappa l_{\rm sonic}$ was important for relating the mathematical properties of the model to physical characteristics of the turbulent density field. To test this, we measure $r_{\rm shock}$ from simulation and compare this to $\kappa l_{\rm sonic}$. While not technically a test of the model, this is important to verifying that κ, as measured from the intermittency of the PDF through T, is broadly consistent with the true width of shock structures. In other words, having seen in Sec. 4 that the model gives decent predictions of turbulent statistics, is our physical interpretation $\kappa \sim r_{\rm shock}/l_{\rm sonic}$ consistent with the properties of shocks seen in simulations?

The Lagrangian nature of the GIZMO code implies that the density is directly proportional to the number density of cells. We thus use a simple counting method to measure $r_{\rm shock}$. This involves defining all cells with $\rho > \rho_{\rm max}/10$ (where $\rho_{\rm max}$ is the maximum density across the current snapshot) as being part of a "shock," then counting the number of such cells within radius r, $N_<(r)$, of a randomly chosen center cell. Ideally, if $r < r_s$, then $N_<(r) \sim r^3$, while if $r > r_s$ then $N_<(r) \sim r^\upsilon$, where $\upsilon \approx 2$ is the fractal dimension of the shock (Federrath et al. 2008). We carry out this procedure for 10000 randomly chosen center cells per simulation, averaging

the results, then averaging these results over time in the statistical steady state of the turbulence. Of course, in the messiness of a true turbulent density field, the transition at $r \sim r_s$ will be relatively smooth, and it is difficult to unambiguously define r_{shock}. In addition, at very small scales $N_<(r)$ is adversely affected by the finite number of cells, since $N_<(r) \to 1$ as $r < r_{cell}$ (where r_{cell} is the size of a cell in the shocked region). Note that this method assumes an approximately constant distribution of cells inside the shock, which appears to be the case based on examination of 2-D density field slices.

Results are shown in Fig. B1 for the $\mathcal{M} \approx 12$ and $\mathcal{M} \approx 7$ simulations from above. In both cases there is a clear flattening to $N_<(r) \sim 2$ (the further flattening at higher r is probably related to the finite extent of the nearly 2-D high density regions). The key point is that this flattening occurs well below $r \sim l_{sonic} = \mathcal{M}^{-2}$, in approximate agreement with the estimate $r \sim \kappa l_{sonic}$ with $\kappa \sim 0.2$. Thus, while it is difficult to accurately measure the shock width, our hypothesis that $r_{shock} \sim \kappa l_{sonic}$ is consistent with the data, while $r_{shock} \sim l_{sonic}$ provides a significant overestimate of the width. Future simulations at higher resolution may allow for a more accurate determination of these properties, by more accurately capturing the transition from supersonic to subsonic motions and allowing measurements over a wider range of $\mathcal{M}$. Unfortunately, even with the Lagrangian numerical method, the shock size at $\mathcal{M} \approx 40$ is still too small to see a transition from $N_<(r) \sim r^2$ to $N_<(r) \sim r^3$ (i.e., $r_{cell} < r_{shock}$), so we do not plot this here.

REFERENCES

Aluie, H. 2011, Phys. Rev. Lett., 106, 174502

Audit, E., & Hennebelle, P. 2005, Astron. Astrophys., 433, 1

Banerjee, R., Vázquez-Semadeni, E., Hennebelle, P., & Klessen, R. S. 2009, Mon. Not. R. Astron. Soc., 398, 1082

Banerjee, S., & Galtier, S. 2013, Phys. Rev. E, 87, 013019

Bauer, A., & Springel, V. 2012, Mon. Not. R. Astron. Soc., 423, 3102

Boldyrev, S. 2002, Astrophys. J., 569, 841

Burkhart, B., Falceta-Gonçalves, D., Kowal, G., & Lazarian, A. 2009, Astrophys. J., 693, 250

Castaing, B. 1996, J. Physique II, 6, 105

Cho, J., & Lazarian, A. 2003, Mon. Not. R. Astron. Soc., 345, 325

Crutcher, R. M. 1999, Astrophys. J., 520, 706

Crutcher, R. M., Wandelt, B., Heiles, C., Falgarone, E., & Troland, T. H. 2010, Astrophys. J., 725, 466

Davidson, P. A. 2015, Turbulence, An Introduction for Scientists and Engineers (Oxford University Press)

Dehnen, W., & Aly, H. 2012, Mon. Not. R. Astron. Soc., 425, 1068

Draine, B. T. 2003, Ann. Rev. Astron. Astrophys., 41, 241

Dubrulle, B. 1994, Phys. Rev. Lett., 73, 959

Federrath, C. 2013, Mon. Not. R. Astron. Soc., 436, 1245

Federrath, C., & Banerjee, S. 2015, Mon. Not. R. Astron. Soc., 448, 3297

Federrath, C., & Klessen, R. S. 2012, Astrophys. J., 761, 156

Federrath, C., Klessen, R. S., & Schmidt, W. 2008, Astrophys. J. Lett., 688, L79

Federrath, C., Roman-Duval, J., Klessen, R. S., Schmidt, W., & Mac Low, M. M. 2010, Astron. Astrophys., 512, A81

Gazol, A., & Kim, J. 2013, Astrophys. J., 765, 49

He, G., Dubrulle, B., & Graner, F. 1998, Phys. Lett. A, 245, 419

Hennebelle, P., & Chabrier, G. 2013, Astrophys. J., 770, 150

Hopkins, P. F. 2013a, Mon. Not. R. Astron. Soc., 430, 1653

—. 2013b, Mon. Not. R. Astron. Soc., 430, 1880

—. 2015a, Mon. Not. R. Astron. Soc., 450, 53

—. 2015b, Mon. Not. R. Astron. Soc., 455, 89

Hopkins, P. F., & Lee, H. 2016, Mon. Not. R. Astron. Soc., 456, 4174

Hopkins, P. F., & Raives, M. J. 2016, Mon. Not. R. Astron. Soc., 455, 51

Kim, J., & Ryu, D. 2005, Astrophys. J., 630, L45

Kolmogorov, A. 1941, Akademiia Nauk SSSR Doklady, 30, 301

Konstandin, L., Girichidis, P., Federrath, C., & Klessen, R. S. 2012, Astrophys. J., 761, 149

Konstandin, L., Schmidt, W., Girichidis, P., Peters, T., Shetty, R., & Klessen, R. S. 2016, Mon. Not. R. Astron. Soc., 460, 4483

Kowal, G., Lazarian, A., & Beresnyak, A. 2007, Astrophys. J., 658, 423

Kritsuk, A. G., Norman, M. L., Padoan, P., & Wagner, R. 2007, Astrophys. J., 665, 416

Krumholz, M. R., & McKee, C. F. 2005, Astrophys. J., 630, 250

Lee, H., Hopkins, P. F., & Squire, J. 2016, arXiv:1612.05264

Lemaster, M. N., & Stone, J. M. 2008, Astrophys. J. Lett., 682, L97

Lithwick, Y., & Goldreich, P. 2001, Astrophys. J. Lett., 562, 279

Mallet, A., & Schekochihin, A. A. 2017, Mon. Not. R. Astron. Soc., 466, 3918

Molina, F. Z., Glover, S. C. O., Federrath, C., & Klessen, R. S. 2012, Mon. Not. R. Astron. Soc., 423, 2680

Padoan, P., & Nordlund, A. 2011, Astrophys. J., 730, 40

Padoan, P., Nordlund, A., & Jones, B. J. T. 1997, Mon. Not. R. Astron. Soc., 288, 145

Pan, L., Padoan, P., Haugbølle, T., & Nordlund, Å. 2016, Astrophys. J., 825, 30

Passot, T., & Vázquez-Semadeni, E. 1998, Phys. Rev. E, 58, 4501

Price, D. J., & Federrath, C. 2010, Mon. Not. R. Astron. Soc., 406, 1659

Price, D. J., Federrath, C., & Brunt, C. M. 2011, Astrophys. J. Lett., 727, L21

Saichev, A. I., & Woyczynski, W. A. 1996, SIAM J. App. Math., 64, 1008

Schmidt, W., Federrath, C., Hupp, M., Kern, S., & Niemeyer, J. C. 2009, Astron. Astrophys., 494, 127

She, Z.-S., & Leveque, E. 1994, Phys. Rev. Lett., 72, 336

She, Z. S., & Waymire, E. C. 1995, Phys. Rev. Lett., 74, 762

Stewart, T., Strijbosch, L., Moors, J., & P., B. 2006, A simple approximation to the convolution of gamma distributions. Discussion Paper, Tilburg University, Center for Economic Research